Effects of ignition location on CH_4/air explosion characteristic in a spherical bomb

Chao Li [a,b], Baiwei Lei [a,b,*], Renhua Pang [a,b], Jianjun Xiao [c], Mike Kuznetsov [c], Thomas Jordan [c]

[a] School of Emergency Management and Safety Engineering, China University of Mining & Technology (Beijing), Beijing 100083, China
[b] Institute for Emergency Rescue Ergonomics and Protection, China University of Mining and Technology (Beijing), Beijing 100083, China
[c] Institute of Thermal Technologies and Safety, Karlsruhe Institute of Technology, Eggenstein-Leopoldshafen 76344, Germany

Keywords:
CH_4/air mixture
Ignition location
Peak pressure
Heat loss
GASFLOW-MPI

A B S T R A C T

To build methane anti-explosion storage equipment, the influence of the ignition location on the CH_4/air explosion in a spherical equipment was investigated. A two-step CH_4/air reaction mechanism was developed and it considered the effect of heat transfer on the explosion. The effect of methane explosion pressure on heat loss was studied. The results show that the maximum explosion pressure of central ignition is 0.72 MPa under the heat loss simulation. The peak pressure of the upper and lower end-wall explosion is about 79.2 % and 83.3 % of the central ignition explosion, respectively, and the experimental results verifies the simulation results. Therefore, the reason for the highest peak pressure of central ignition methane explosion is that the reaction speed of central ignition methane explosion is the fastest, and the heat loss is the lowest. The difference in peak pressure between the upper and lower wall surfaces is due to the buoyancy effect accelerates the reaction rate of the lower end-wall ignition. In the simulation time range, the heat radiation at different ignition locations accounts for more than 70 % of the total heat loss, and radiation heat transfer plays a leading role in the total heat loss.

1. Introduction

Methane is an essential component of natural gas and a promising clean energy source [1–3]. However, it is a flammable and explosive gas, which can lead to fires during industrial transportation and storage. Methane explosion in confined spaces or vessels occur, resulting in severe damage to industrial equipment such as closed vessels for storing methane and causing casualties [4,5]. The construction of process equipment that can withstand the pressure of methane explosions can reduce the risk of casualties and minimize accidents. As a result, before considering application in the industrial field, the explosion characteristics of methane under closed conditions should be investigated. To build process equipment capable of withstanding explosion pressure, it is essential to understand methane explosion characteristics in a closed vessel [6–10]. The ignition position has a significant impact on explosion overpressure and it is closely related to the extent of explosion damage. Therefore, studying the influence mechanism of ignition position on the explosion characteristics of methane is of great significance for the design of combustible gas storage containers and the safe and efficient utilization of clean energy.

The ignition location in spherical equipment affects the reaction process of combustible gas. Researchers have carried out experimental studies [11–15]. The experimental results show that the central ignition explosion will produce the highest maximum peak pressure, and the wall ignition explosion reaction is weak. According to the findings of many researchers [16–19], this is mainly due to the differences in heat losses during gas explosion, and the ignition location can affect the development of explosion and the heat loss during the reaction process [20]. As the heat loss process includes two mechanisms of radiative heat transfer and convective heat transfer [18,19], due to the lack of corresponding experimental measurements in the testing process, the above researchers only qualitatively analyze the heat loss during the ignition location process, and could not quantitatively analyze the contribution ratio of thermal radiation and thermal convection.

Numerical simulations can quantitatively predict the changes in temperature and flow fields and the contribution of heat loss rates to explain the mechanism of pressure rise [14,21]. Many researchers have compared and analyzed the influence of heat transfer conditions on methane explosion [22–24], but there is a lack of analysis of the effect of ignition location on methane explosion in a spherical bomb. Numerical simulation can quantitatively analyze the heat loss in the methane explosion process, which is of great significance to the methane explosion

* Corresponding author at: School of Emergency Management and Safety Engineering, China University of Mining & Technology (Beijing), Beijing 100083, China.
E-mail address: leibws@cumtb.edu.cn (B. Lei).

process study.

While researchers have conducted numerous studies on the explosion characteristics and heat transfer mechanisms of CH_4/air explosions, there is still a lack of research on the influence mechanism of ignition positions on CH_4/air explosion characteristics. Therefore, the impact of different ignition positions on the peak overpressure, maximum pressure rise rate, and heat transfer mechanisms of methane explosions still need further exploration. In this study, a two-step CH_4/air reaction mechanism was established using the CFD code, and a mathematical model of heat loss was developed. The explosion evolution process of methane in a 20L spherical explosive container was simulated and reproduced through the GASFLOW-MPI. The effects of different ignition locations on the characteristics of methane explosion was analyzed, and the variations in the heat transfer mechanism during the methane explosion process was investigated. This study uncover the effects mechanism of heat loss on the overpressure of methane explosions. This research provides a scientific reference for the safe and efficient utilization of fuel (CH_4) and the design of closed pressure vessels.

2. Numerical model

GASFLOW-MPI is a CFD code specifically designed for the safety analysis of combustible gases. It can solve three-dimensional compressible Navier–Stokes equations. In our earlier work, the reliability of GASFLOW-MPI in predicting the combustion and explosion of premixed combustible gases (such as methane [24–27] and hydrogen [28–31]) has already been demonstrated. This section introduces the governing equations for the explosion of premixed combustible gases (CH_4) and the two-step combustion reaction mechanism.

2.1. Conservation equation

The mass, momentum, and energy conservation equations for mixed gas can be expressed as follows [32,33]:

$$\frac{d}{dt}\int_V \rho dV = \oint_S \rho u dS + \int_V S_{\rho,com} dV \tag{1}$$

$$\frac{d}{dt}\int_V \rho_\alpha dV = \oint_S [\rho_\alpha u + J_\alpha] dS + \int_V S_{\rho,\alpha,com} dV \tag{2}$$

$$\frac{d}{dt}\int_V \rho u dV = \oint_S [\rho uu \quad P \quad \tau] dS + \int_V \rho g dV \tag{3}$$

$$\frac{d}{dt}\int_V \rho I dV = \oint_S [\rho Iu \quad Pu \quad q] dS + \int_V \left(S_{I,com} + S_{I,conv} + S_{I,rad} + S_{I,cond}\right) dV \tag{4}$$

where u represents the mean velocity, $S_{I,com}$ represents the source of energy produced by explosion, V represents the volume, P represents the pressure, $S_{\rho,com}$ represents the mass source term, S represents the control surface; α represents the gas specie, τ represents the stress tensor, ρ_α represents the density, J_α represents the diffusion term of specie α, and $S_{\rho,\alpha,com}$ represents the mass change of gas explosion, $S_{I,rad}$ represents the radiation mechanism, g represents the gravitational acceleration, $S_{I,rad}$ represents the steam condensation, and $S_{I,conv}$ represents the convection mechanism.

2.2. Turbulence model

Detached eddy simulation (DES) turbulence model has been successfully applied in numerous industrial cases. Zhang et al. validated the computational accuracy of the DES turbulence model [34]. Therefore, in this study, the DES turbulence model was chosen.

2.3. Reaction mechanism

Assuming the methane explosion process involves two-step chemical reactions [35,36]:

$$CH_4 + 1.5O_2 \rightarrow CO + 2H_2O \tag{5}$$

$$CO + 0.5O_2 \leftrightarrow CO_2 \tag{6}$$

For the methane–oxygen reactions in Eq. (5) and Eq. (6), the reaction can be expressed as follows [35]:

$$\dot{\omega}_{f,1} = k_{f,1}(T) C_{CH_4}^{0.5} C_{O_2}^{0.65} \tag{7}$$

$$\dot{\omega}_{f,2} = k_{f,2}(T) C_{CO} C_{O_2}^{0.5} \tag{8}$$

where the rate constant $k(T)$ is independent of the concentration and varies with temperature. The rate constant is modeled by implementing a modified Arrhenius law in the following form:

$$k_{f,1}(T) = f_1(\phi) C_{f,1} T^{n1} e^{\left(-E_{a,1}/RT\right)} \tag{9}$$

$$k_{f,2}(T) = f_2(\phi) C_{f,2} T^{n2} e^{\left(-E_{a,2}/RT\right)} \tag{10}$$

where C_f denotes the frequency factor (in this model, $C_{f,1}$=4.9 × 10^9 and$C_{f,2}$ = 2 × 10^8), n is the temperature exponent (in this model, $n1$ = 0 and$n2$ = 0.8), E_a represents the activation energy ($E_{a,1}/R$=1.78772 × 10^4 K and$E_{a,2}/R$ = 0.6043 × 10^4 K), and $f_i(\phi)$ are correction functions. The specific formula is in [35,37].

2.4. Heat transfer model

In the process of a methane explosion in a spherical bomb, there is a heat transfer phenomenon between the fluid and the wall surface. Therefore, we established a heat transfer model of spherical bomb explosion, divided into convective heat transfer [38,39] and radiation heat transfer [30,39]. The asymmetric molecules in the explosion products during the explosion are the primary sources of thermal radiation, such as water vapor and carbon dioxide [30,40–43].

3. Modeling of the 20 L spherical bomb

3.1. Geometric modeling

Fig. 1 shows a 20 L spherical bomb experimented on by Luo et al. [45]. The 20 L spherical bomb has an outer diameter of 36 cm and a wall

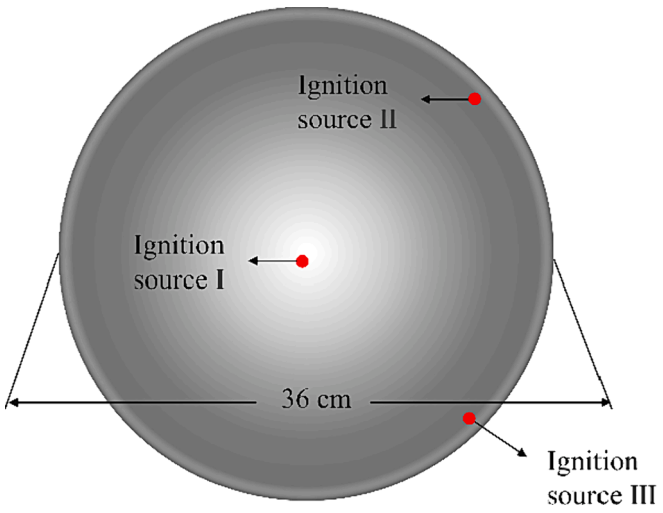

Fig. 1. Schematic diagram of a 20 L spherical bomb. (I: central ignition, II: upper end-wall ignition, III: lower end-wall ignition).

thickness of 1 cm. Fig. 2 (a) and Fig. 2 (b) are schematic diagrams of the experimental central ignition location and the upper end-wall ignition location, respectively. In this study, the lower wall ignition location was added to compare the effects of different sidewall ignition locations on the methane explosion characteristics, as shown in Fig. 2 (c).

3.2. Numerical simulation set-up

Luo et al. [45] and their research group [46] used stainless steel as the primary material for the spherical bomb. The specific parameters for numerical simulation modeling were modeled based on the descriptions of the physical properties of stainless steel by Lei et al. [24] and the Engineering ToolBox [47], as well as experimental environmental conditions [44,45], as shown in Table 1. To ensure calculation accuracy, meshes are set in the computational domain to improve computational efficiency. The total number of meshes in the simulation is 148,877, and the number of meshes in the three directions of the x, y, and z axes is 53. The three-dimensional grid is a small cube with side lengths of 6.6 mm. In this paper, to verify the independence of the mesh, the mesh side length of the 20 L spherical explosion bomb geometric model is divided into 6.6 mm and 3.3 mm. Fig. 3 shows the pressure change curves of spherical bombs at different ignition locations under the two grid side lengths. When the number of grids at each ignition location is 148877, the pressure change in the spherical bomb is similar to that of the 297,757 grids. Due to the good convergence of the results, 148,877 mesh numbers were chosen for this study to save simulation time.

4. Discussion

4.1. Data validation analysis

To validate the accuracy of numerical simulation results, the 9.5 % methane explosion experimental data of the upper end-wall ignition [44] and central ignition [45] were compared with the numerical simulation results. Both sets of experimental data were measured in a 20 L spherical bomb, as shown in the figure. Fig. 4 (a) compares the pressure–time curves of experimental and simulated results for central ignition. its evident that simulation results exhibits good consistency with the experimental results. In addition, Fig. 4 (b) and (c) compare the numerical simulation and experimental data for the central and upper end-wall ignition. The peak pressure P_{max}, time to reach the peak pressure t, and maximum pressure rise rate $(dp/dt)_{max}$ calculated by GASFLOW-MPI code are similar to the experimental results and have errors of 4.17 %, 3.33 %, and 6.45 %, respectively. The calculation results agree with the experimental results, proving that the numerical simulation results are reliable and effective.

Table 1
Simulation of detailed parameter settings.

Items	Value
Initial ambient temperature	298 K
Gravity acceleration	9.8 m/s^2, along the negative direction of the z-axis
Explosion bomb wall material	Stainless steel
Methane concentration	9.5 %
Atmospheric pressure	0.1 MPa
Wall material density	7850 kg/m^3
Specific heat capacity under constant pressure	490 J/kg·K
Wall material emissivity	0.85
Thermal conductivity	50 W/m·K

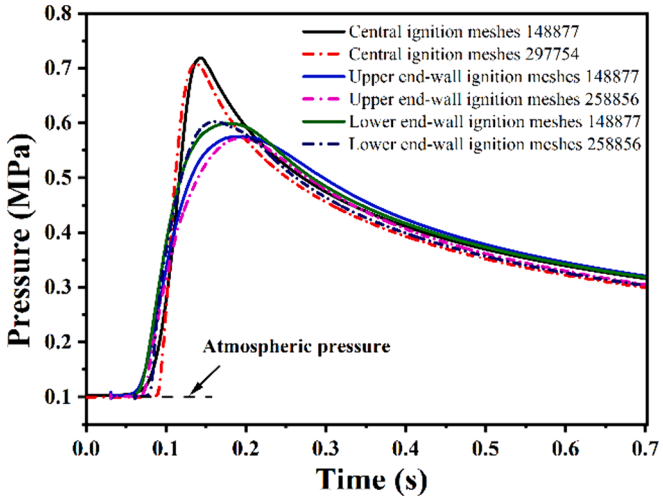

Fig. 3. Mesh independence test for different ignition locations.

4.2. Explosion pressure

The curves of the explosion pressure P and pressure rise rate dp/dt over time at different ignition locations simulated by adiabatic simulation and simulated calculations considering heat loss are shown in Fig. 5. Fig. 5 (a) shows that under adiabatic conditions, P_{max} at different ignition locations are equal. However, the times required to reach P_{max} are different. The central ignition explosions were approximately 53 % and 40 % faster than the upper and lower end-wall ignition. Fig. 5 (b) shows the corresponding dp/dt curve. The rising rate of the ignition pressure on the lower wall first increases, which also corresponds to an increase in the ignition pressure curve on the lower wall in the enlarged area of Fig. 5 (a). $(dp/dt)_{max}$ of the central ignition is 22.19 MPa/s, which is

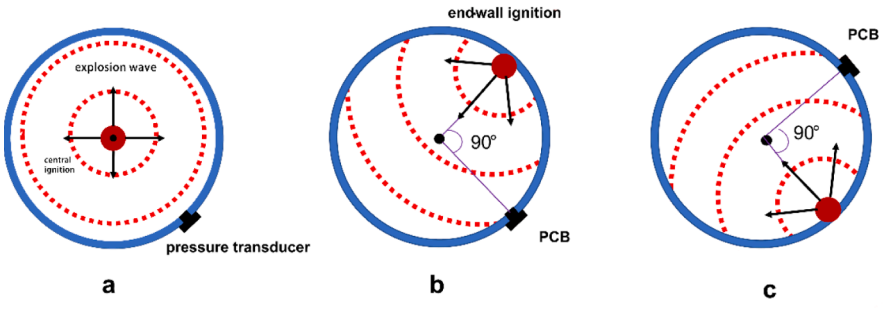

(a) central ignition (b) upper end-wall ignition (c) lower end-wall ignition

Fig. 2. Schematic diagram of the methane explosion reflected wave with different ignition positions.

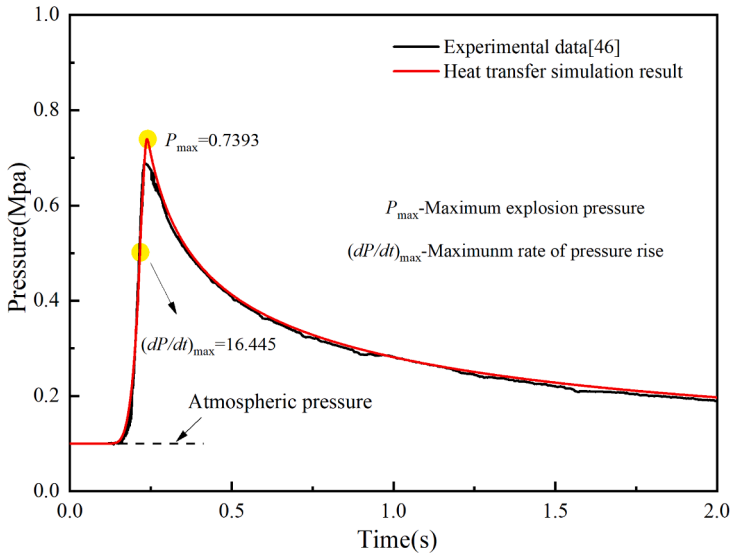

(a) Pressure curves for central ignition experiments and numerical simulations

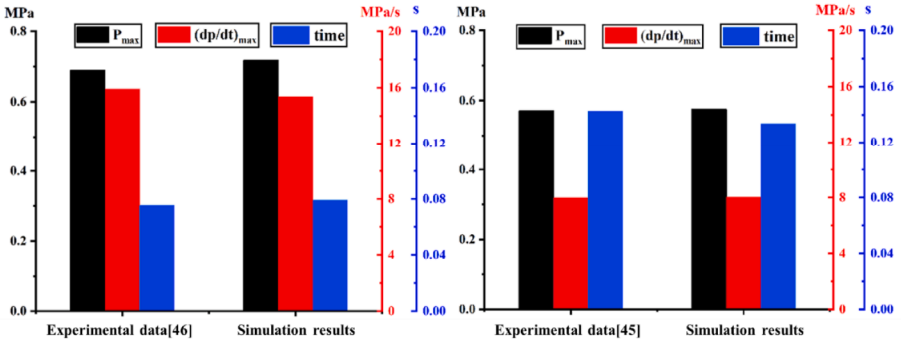

(b) central ignition (c) upper end-wall ignition

Fig. 4. Comparison chart of 9.5% CH_4 explosion experimental data and numerical simulation results (where $(dp/dt)_{max}$ represents the maximum pressure rise rate; P_{max} represents the peak pressure; t represents the time to reach the peak pressure).

more than 60 % higher than that of the end-wall ignition. According to the isothermal model [48], dp/dt as Eq. (11), dp/dt is related to the flame front area A and laminar burning velocity K_r. Under static conditions, the flame front area of the central ignition explosion is more significant than that of the end-wall ignition. Therefore, $(dp/dt)_{max}$ of the central ignition is higher than the end-wall ignition. $(dp/dt)_{max}$ of the lower end-wall ignition is slightly higher than that of the upper end-wall ignition due to the buoyancy effect [49] that accelerates the explosion rate of methane.

$$\frac{dP}{dt} = \frac{\alpha K_r A P(P_m \quad P)}{V P_0} \tag{11}$$

where P_0 represents the initial pressure, α means the turbulence factor. When there is no turbulence, α=1, P represents the measured pressure, A denotes the flame front area, P_m represents the final (and maximum) pressure, K_r denotes the laminar burning velocity, V represents the volume of the facility.

The peak pressure calculated by considering the heat loss simulation was lower than the adiabatic simulation, especially where the end-wall ignition explosion was obvious. As shown in Fig. 5 (c), P_{max} of the central ignition methane explosion was 0.72 MPa, and those of the upper and lower end-wall ignition explosions were approximately 79.2 % and 83.3 % of the central ignition explosion. However, the downward trend of dp/dt was similar to that of the adiabatic simulation. In Fig. 5 (d), although $(dp/dt)_{max}$ of the upper and lower end-wall ignition fluctuated, the downward trends were consistent. The time when the ignition explosion dp/dt of the upper and lower end-walls reached the peak corresponding to the time of the temperature cloud map. The distances of the flame front in Fig. 6 were 0.30949 m and 0.31766 m, which implied that it was the other end of the explosion bomb. From the temperature cloud diagram in Fig. 5 (d), it can also be seen that for the explosion of a uniformly mixed CH_4/air mixture in the explosion device, the junction of the purple and red temperature gradients can indicate the flame front location. That is, the flame generated by the explosion reaches the other end of the explosion bomb at 0.094 and 0.088 s, filling the entire explosion device. Thus, causing the subsequent downward trend of dp/dt of the two end-wall ignitions coincides. As shown in Fig. 6, the flame front velocity of end-wall ignition explosion is much faster than that of central ignition. This is because the end-wall ignition explosion gas only expands to one side, while the central ignition expands to all sides, so the flame front propagation velocity is slower and more stable.

4.3. *Temperature and flow field*

Fig. 7 shows the evolution of the spatial distribution of the explosion temperature and gas velocity at different ignition locations. At the beginning of the explosion, the lower end-wall ignition explosion first began to react when the explosion bomb gas from the lower end-wall

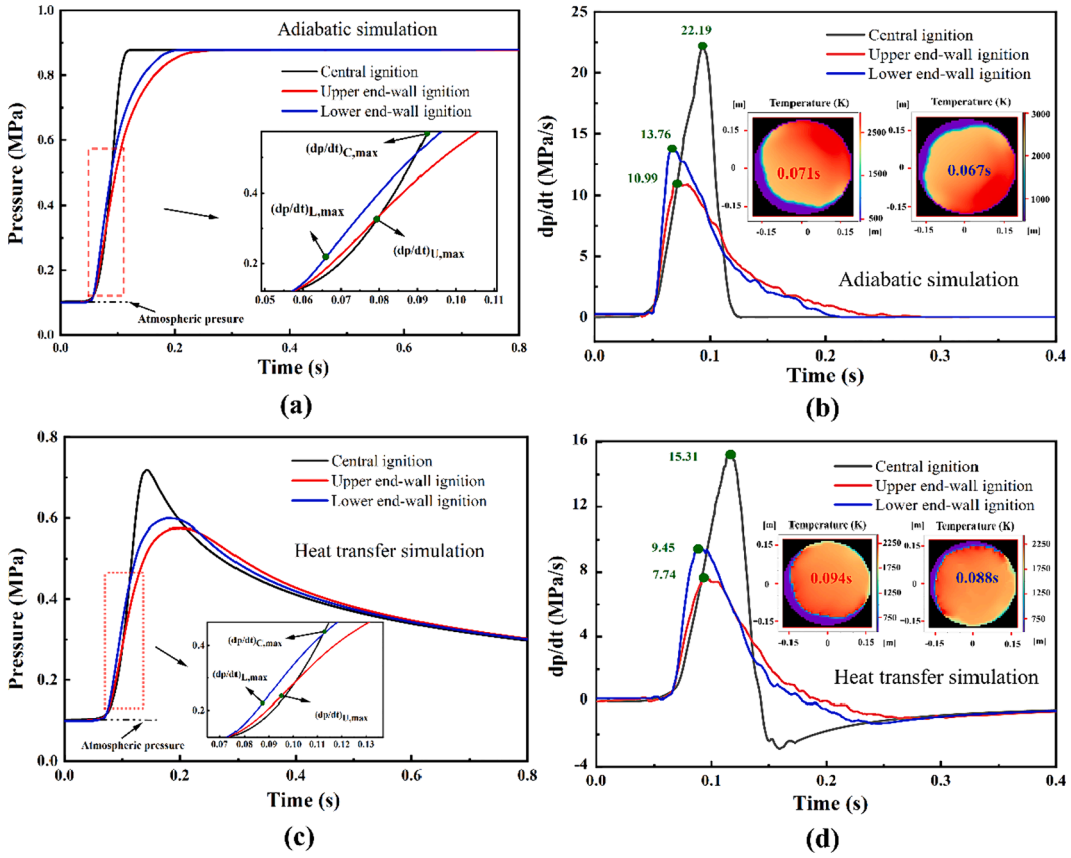

Fig. 5. Methane explosion pressure (a, c) and pressure rise rate evolution over time (b, d).

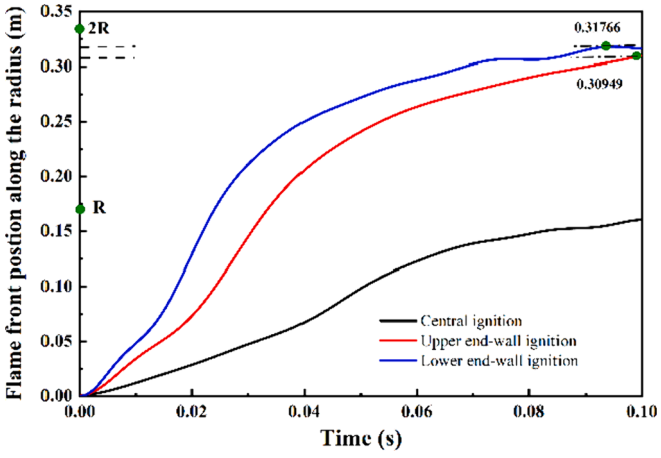

Fig. 6. Flame front location along the radius evolution over time.

had a hemispherical outward flow at a maximum gas flow rate of 4 m/s. At 50 ms, the central ignition explosion temperature began spreading outward from the ignition center, the lower end-wall ignition explosion temperature spread more than half of the volume of the explosion device, and the gas reached the distal wall and reflection. At the 100 ms, the upper and lower end-wall flow fields are centered on the line between the ignition location and the center of the ball, forming two opposite vortices on the upper and lower sides of the oblique. At 180 ms, the temperature in the explosion device gradually decays owing to the wall thermal reaction [50], and the temperature at the wall ignition is significantly lower than that at the far wall. Under the double driving force of explosion and buoyancy, the central ignition explosion forms an updraft in the ignition center area, reaching the arc top of the spherical airtight bomb and splitting to both sides. Two opposite vortices are formed on both sides, and the high-temperature airflow converges at the bottom. Thus, the base temperature of the center ignition explosion bomb is higher than the top temperature at 180 ms.

4.4. *Gas concentration*

The variation curves of the gas concentration and temperature of the methane explosion at different ignition locations are shown in Fig. 8. From comparing the methane concentration decline curves of the three ignition locations, it can be seen that methane in the central ignition explosion first reacts and the temperature of the explosion bomb also reaches a peak of 2159 K. Because the methane explosion simulation was set as a two-step reaction, 0.0106 % carbon monoxide was produced. Compared with the center of the explosion, end-wall ignition is in contact with less oxygen and has an inadequate reaction, resulting in increased carbon monoxide production, namely the volume fraction of carbon monoxide produced is 26.1 % and 7.2 % more than central ignition, respectively. There is also a slight difference in the peak temperature between the upper and lower end-wall ignition because the lower end-wall ignition burns faster than the upper end-wall ignition due to buoyancy. The flame front contacts the fresh air earlier, the reaction is more sufficient, and less carbon monoxide is produced.

Fig. 9 shows that the methane consumption rate of the central ignition increases rapidly to a peak of 0.0287 kg/s within 0.08 s, which indicates that the flame of the central ignition explosion expands quickly and the consumption rate is higher than that of the end-wall ignition explosion. For the upper and lower end-wall ignition, the methane consumption time of the lower end-wall ignition is approximately 39 % shorter than that of the upper end-wall ignition. Because of the effect of buoyancy, the propagation speed of the lower end-wall ignition flame

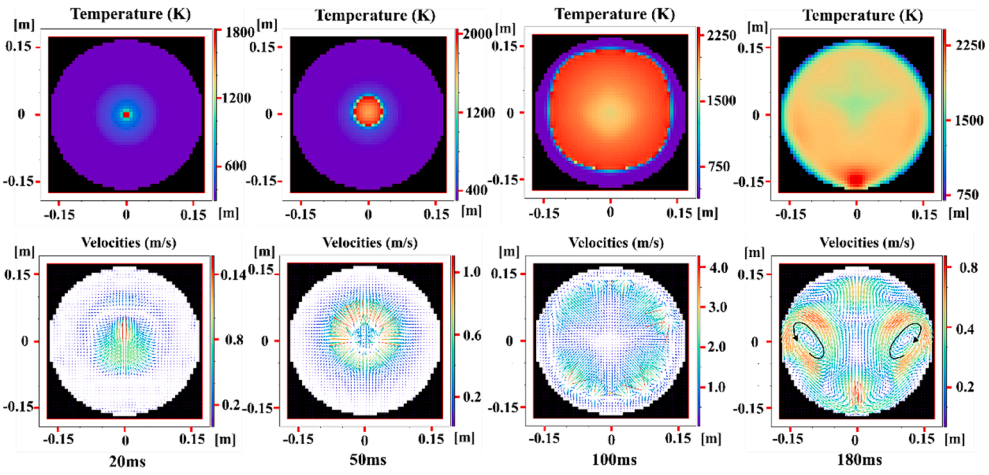

(a) Central ignition

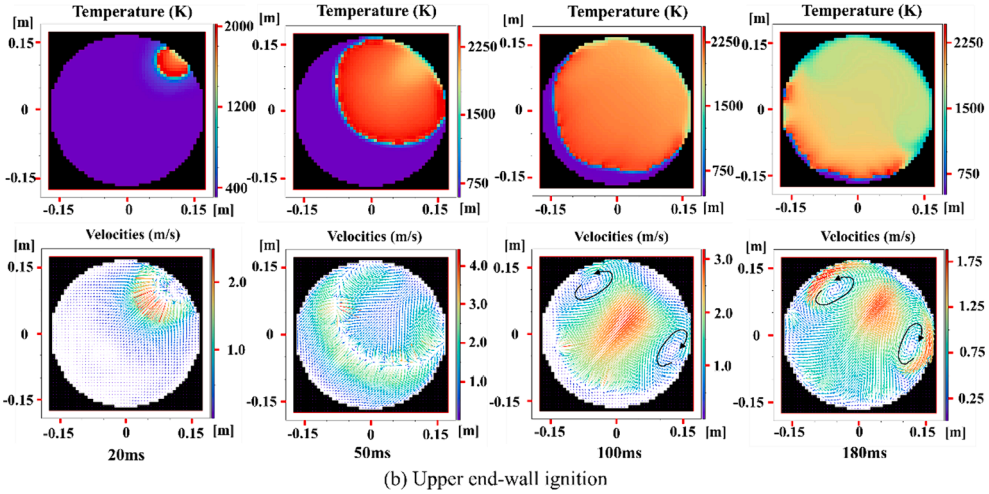

(b) Upper end-wall ignition

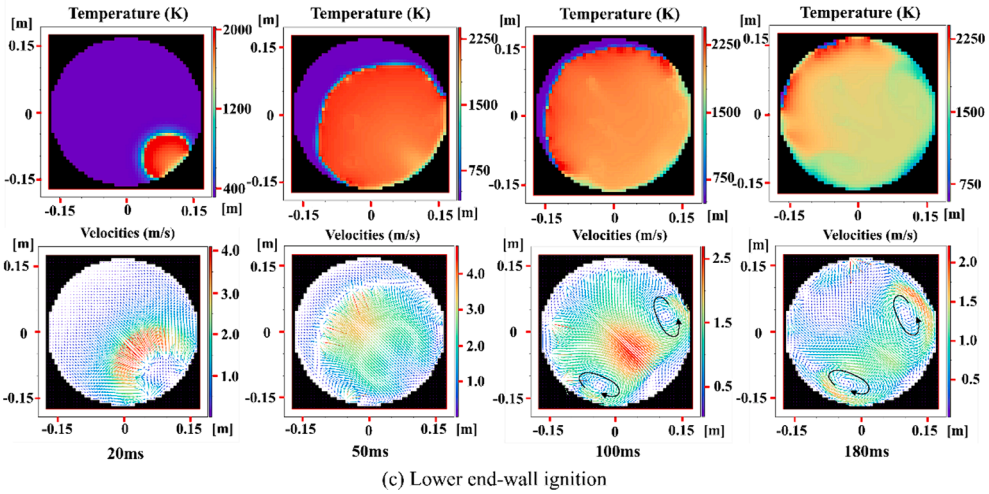

(c) Lower end-wall ignition

Fig. 7. Cloud image of 9.5 % CH_4/air calculated explosion: (a) central ignition, (b) upper end-wall ignition, and (c) lower end-wall ignition.

front is faster. Thus, the flame generated by the explosion expanded to the unburned area more quickly, resulting in speedier methane consumption.

4.5. *Heat loss analysis*

The heat generation and release law of methane explosion under the condition of heat transfer in the explosion bomb were analyzed. Fig. 10 shows the curves depicting the variations in heat release, heat loss, and heat transfer mechanisms during the methane explosion process are illustrated. As shown in Fig. 10 (a), According to the Eq. (12), it can be determined that H_r of the central ignition explosion reaches a maximum at 134 ms, which is 297 kJ/s, and the peak heat loss rates of the upper and lower end-wall ignition explosions are only 173 kJ/s and 191 kJ/s,

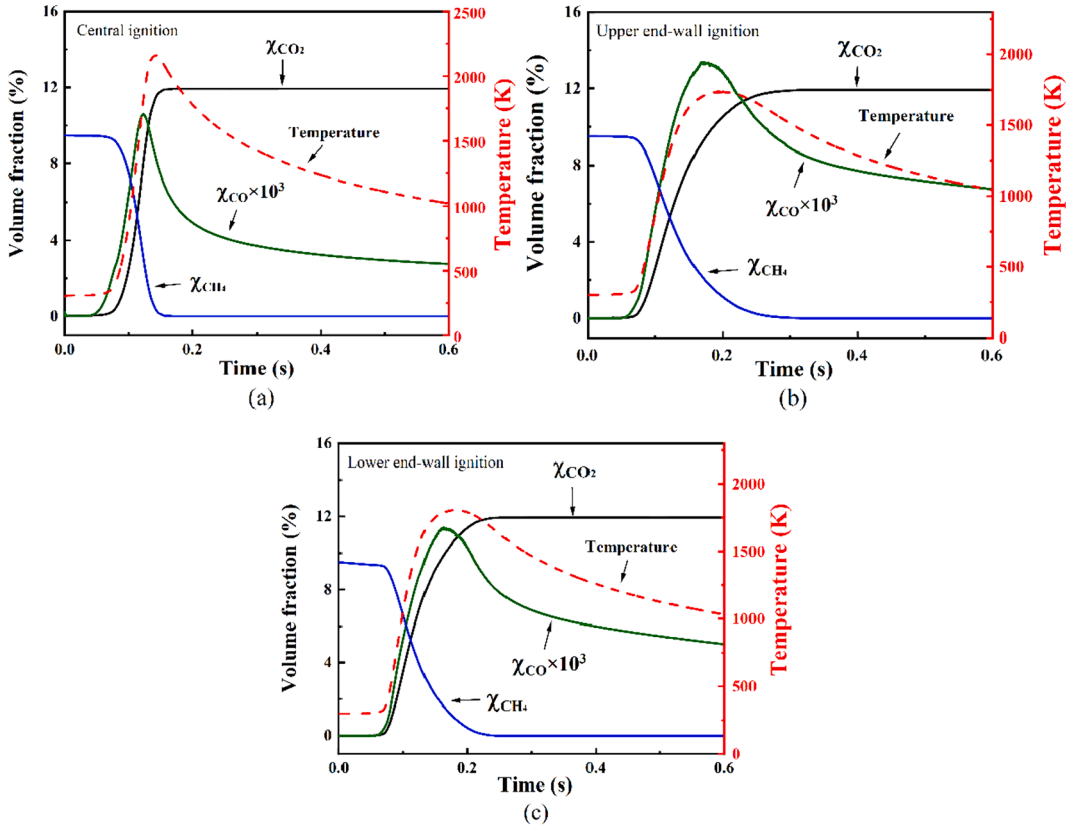

Fig. 8. Gas components and temperature evolution over time.

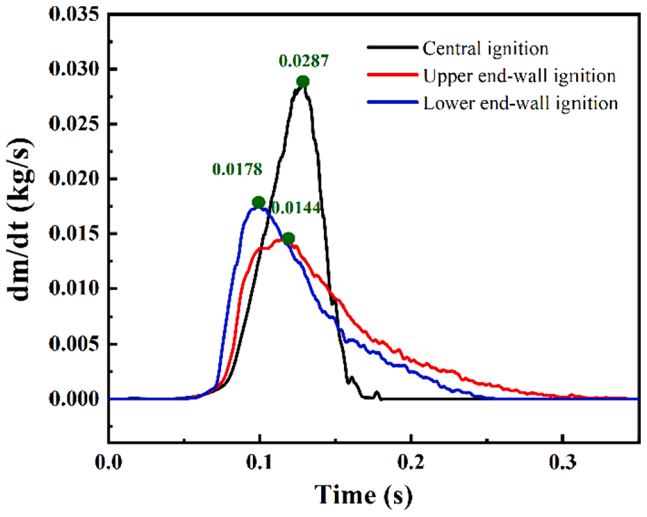

Fig. 9. Methane mass consumption rate (dm/dt) evolution over time.

respectively. By comparison, the peak heat loss rate of the central ignition is more significant, and the t_h value is smaller. This is because the central ignition explosion quickly spread to the entire explosion bomb, the end-wall was in complete contact with the explosion flame, and the heat loss rate reached its peak. The heat loss rate curve of the end-wall ignition increased earlier because the ignition location was located on the wall surface, the convective heat transfer was substantial, and a considerable amount of explosion energy was consumed. This is the main reason the peak pressure of end-wall ignition explosion is lower than that of central ignition [51]. As shown in Fig. 10 (a), 10 (c), and 10 (e), when the explosion reaches the peak pressure, the total heat release and loss of the central ignition are 60.1 kJ and 10.8 kJ, respectively, and the residual heat of the explosion bomb is 49.3 kJ. Under this condition, the residual heat of the upper and lower end-wall ignition is 38 kJ and 40 kJ, respectively, 77 % and 81 % of the central ignition. P_{max} of the upper and lower end-wall ignition are 79.2 % and 83.3 % of the central ignition. Therefore, P_{max} of the end-wall ignition explosion is lower than that of the central ignition because of the heat difference in the explosion device, that is, the heat loss is different.

$$Q = H_r \cdot t \tag{12}$$

where Q represents the total heat loss, t represents the heat-loss time during explosion, H_r represents the heat-loss rate.

Heat loss occurs in the explosion bomb explosion, considering heat loss simulation. The relative contributions of the radiative and convective heat transfer mechanisms to the heat loss at each ignition location are shown in Fig. 10 (b), 10 (d), and 10 (f). The central ignition explosion is dominated by radiation heat transfer in stage I, and the convective heat transfer gradually increases, whereas the end-wall ignition has a higher convective heat transfer in stage I. At 0.8 s, the contributions of heat radiation to heat loss are 72.98 %, 73.51 %, and 72.77 % when the central, upper, and lower end-walls are ignited. Overall, although the proportion of convective heat transfer increases over the simulation time range, the thermal radiation at each ignition location accounted for more than 70 % of the total heat loss. Therefore, radiation heat transfer is the primary form of heat loss during the methane explosion process.

5. Conclusions

A two-step CH_4/air reaction mechanism was established based on a CFD code. The impact of different ignition positions on the explosion characteristics of CH_4/air was studied in a 20L explosion sphere. Combining heat transfer mechanisms, the influence mechanisms of different ignition positions on methane explosion characteristics were

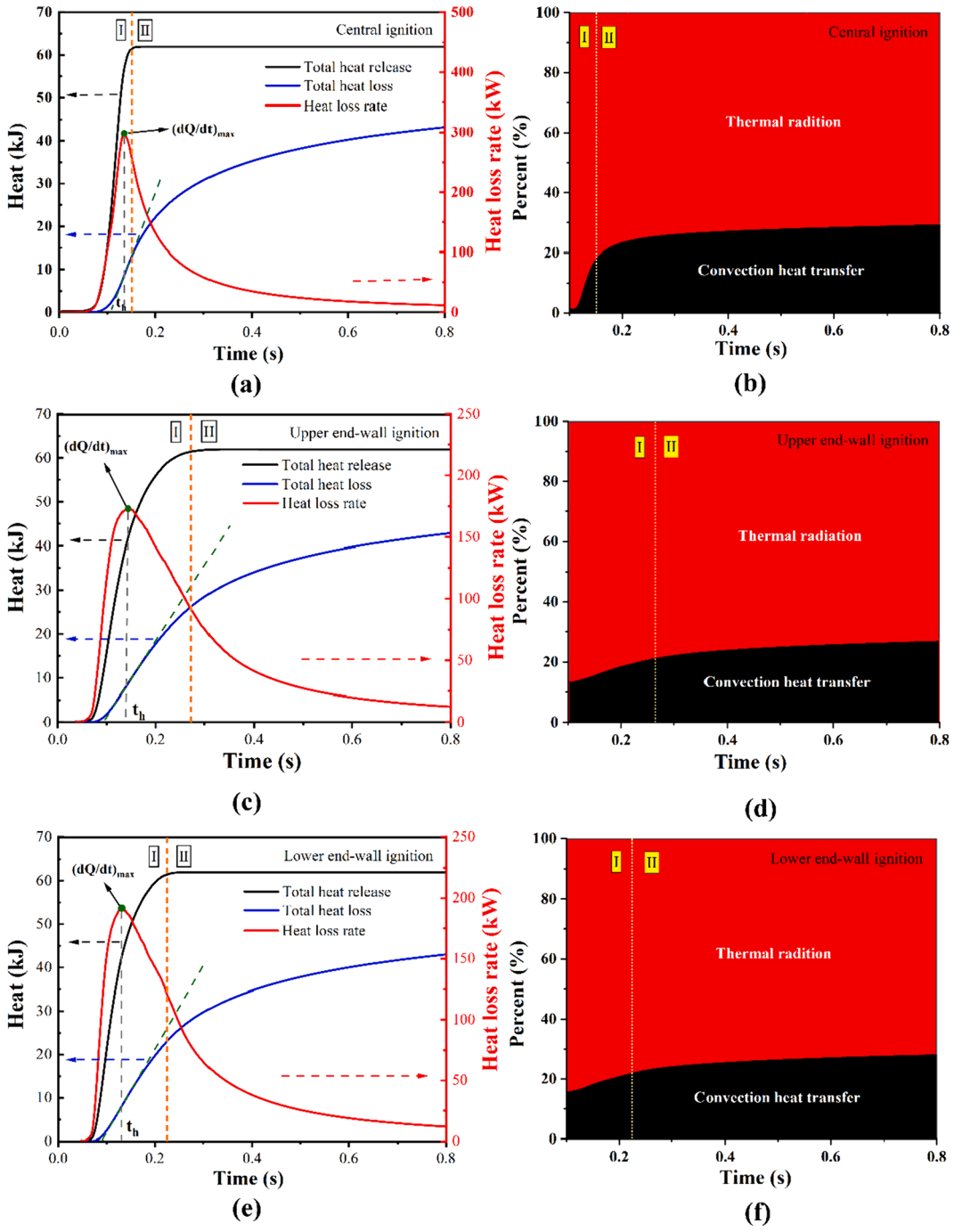

Fig. 10. Heat production and dissipation curve (a, c, and e), the contribution of the heat transfer mechanism (b, d, and f).

revealed. The following conclusions were obtained:

(1) Ignition position has a significant impact on the explosion characteristics of methane. The maximum overpressure and the maximum rate of pressure rise for methane explosions with central ignition are markedly greater than those with end-wall ignition. Explosions with ignition on the upper and lower end-wall ignition respectively contribute to 79.2 % and 83.3 % of the maximum overpressure observed in central ignition explosions. The maximum rate of pressure rise for central ignition is more than 60 % faster than that for end-wall ignition. The buoyancy effect accelerates the methane explosion rate, resulting in lower end-wall ignition explosions having significantly higher overpressure and maximum rate of pressure rise than end-wall ignition and slightly higher than upper end-wall ignition.

(2) Heat loss is a crucial factor influencing the explosion characteristics at different ignition positions, with heat radiation being the primary form of thermal loss. Heat radiation during the explosion processes at various ignition positions accounts for more than 70 % of the total heat loss. The total heat loss during central ignition explosions is the lowest, while the heat loss during explosions with the upper and lower end-wall ignition is approximately twice that of central ignition explosions. Analysis based on the methane explosion energy equation reveals that the difference in heat loss during end-wall ignition explosions is a significant

factor leading to lower maximum overpressure compared to central ignition.

Considering the heat transfer mechanisms and the influence of different ignition positions on explosion characteristics in the design process of combustible gas storage containers in the chemical industry can enhance the accuracy of explosion characteristic parameter assessments. The research outcomes provide a more scientifically grounded assessment approach and reference basis for the design of combustible gas storage containers and the safe and efficient utilization of clean energy in the chemical industry.

CRediT authorship contribution statement

Chao Li: Writing – original draft, Methodology, Conceptualization. **Baiwei Lei:** Writing – review & editing, Validation, Software, Methodology, Methodology. **Renhua Pang:** Writing – original draft, Validation. **Jianjun Xiao:** Writing – review & editing, Software. **Mike Kuznetsov:** Writing – review & editing. **Thomas Jordan:** Writing – review & editing.

Declaration of competing interest

The authors declare that they have no known competing financial interests or personal relationships that could have appeared to influence the work reported in this paper.

Data availability

No data was used for the research described in the article.

Acknowledgements

This work was supported by the National Key R&D Program of China [2023YFB3211001], the National Natural Science Foundation of China [52374252], the Undergraduate Education and Teaching Reform and Research Project of China University of Mining and Technology (Beijing) [J231202] and the Fundamental Research Funds for the Central Universities [2023ZKPYAQ03]. Baiwei Lei was also like to acknowledge China Scholarship Council for its financially supported.

References

[1] X.B. Shen, G.L. Xiu, S.Z. Wu, Experimental study on the explosion characteristics of methane/air mixtures with hydrogen addition, Appl. Therm. Eng 120 (2017) 741–747.
[2] M.G. Yu, X.Y. Wang, K. Zheng, S.X. Han, L. Wang, Investigation of methane/air explosion suppression by modified montmorillonite inhibitor, Process Saf. Environ. Prot 144 (2020) 337–348.
[3] K. Zheng, J.C. Jiang, Z.X. Xing, Y.M. Hao, M.G. Yu, X.F. Yang, Y.W. Tao, Application of large eddy simulation in methane-air explosion prediction using thickening flame approach, Process Saf. Environ. Prot 159 (2022) 662–673.
[4] S. Khakzad, F. Khan, R. Abbassi, N. Khakzad, Accident risk-based life cycle assessment methodology for green and safe fuel selection, Process Saf. Environ. Prot 109 (2017) 268–287.
[5] T. Baalisampang, R. Abbassi, V. Garaniya, F. Khan, M. Dadashzadeh, Modelling an integrated impact of fire, explosion and combustion products during transitional events caused by an accidental release of LNG, Process Saf. Environ. Prot 128 (2019) 259–272.
[6] X.P. Wen, M.G. Yu, W.T. Ji, M. Yue, J.J. Chen, Methane–air explosion characteristics with different obstacle configurations, Int. J. Min. Sci. Technol 25 (2015) 213–218.
[7] T. Wang, Z.M. Luo, H. Wen, F.M. Cheng, J. Deng, J.Y. Zhao, Z.C. Guo, J.J. Lin, K. Kang, W.F. Wang, Effects of flammable gases on the explosion characteristics of CH_4 in air, J. Loss Prev. Process. Ind 49 (2017) 183–190.
[8] S.X. Song, Y.F. Cheng, X.R. Meng, H.H. Ma, H.Y. Dai, J.T. Kan, Z.W. Shen, Hybrid CH_4/coal dust explosions in a 20-L spherical vessel, Process Saf. Environ. Prot 122 (2019) 281–287.
[9] X.Y. Chang, B. Zhang, H.D. Ng, C.H. Bai, The effects of pre-ignition turbulence by gas jets on the explosion behavior of methane-oxygen mixtures, Fuel 277 (2020) 118–190.
[10] K. Wang, M.Q. Su, L.J. Wei, S.N. Chen, X.B. Kong, Y.L. Fang, Effect of initial turbulence on explosion behavior of stoichiometric methane-ethylene-air mixtures in confined space, Process Saf. Environ. Prot 161 (2022) 583–593.
[11] J. Kindracki, A. Kobiera, G. Rarata, P. Wolanski, Influence of ignition position and obstacles on explosion development in methane–air mixture in closed vessels, J. Loss Prev. Process. Ind 20 (2007) 551–561.
[12] F. Cammarota, A.D. Benedetto, P. Russo, E. Salzano, Experimental analysis of gas explosions at non-atmospheric initial conditions in cylindrical vessel, Int. J. Hydrogen Energy 88 (2010) 341–349.
[13] J. Guo, X.X. Sun, S.C. Rui, Y. Cao, K.L. Hu, C.J. Wang, Effect of ignition ignition on vented hydrogen–air explosions, Int. J. Hydrogen Energy 40 (2015) 15780–15788.
[14] Y. Zhang, W.G. Cao, C.M. Shu, M.K. Zhao, C.J. Yu, Z.B. Xie, J.H. Liang, Z.Q. Song, X. Cao, Dynamic hazard evaluation of explosion severity for premixed hydrogen–air mixtures in a spherical pressure vessel, Fuel 261 (2020) 116433.
[15] T.K. Dai, B. Zhang, H. Liu, On the explosion characteristics for central and end-wall ignition in hydrogen-air mixtures: a comparative study, Int. J. Hydrogen Energy 46 (2021) 30861–30869.
[16] A.M. Lipanov, A.V. Aliev, T.A. Bodnar, V.M. Druzhdin-Khodos, L.A. Litvinov, Flame propagation in a closed deformable channel, Combust. Explos. Shock Waves 26 (1990) 273–279.
[17] I. Goldfarb, V. Gol'dshtein, G. Kuzmenko, S. Sazhin, Thermal radiation effect on thermal explosion in gas containing fuel droplets, Combust. Theor. Model 3 (1999) 769–787.
[18] Q. Ye, G.G.X. Wang, Z.Z. Jia, C.S. Zheng, Experimental study on the influence of wall heat effect on gas explosion and its propagation, Appl. Therm. Eng 118 (2017) 392–397.
[19] M. Mitu, V. Giurcan, D. Razus, M. Prodan, D. Oancea, Propagation indices of methane-air explosions in closed vessels, J. Loss Prev. Process Ind 47 (2017) 110–119.
[20] D. Razus, C. Movileanu, V. Brinzea, D. Oancea, Explosion pressures of hydrocarbon–air mixtures in closed vessels, J. Hazard. Mater. 135 (2006) 58–65.
[21] G. Ferrara, A.D. Benedetto, E. Salzano, G. Russo, CFD analysis of gas explosions vented through relief pipes, J. Hazard. Mater. 137 (2006) 654–665.
[22] C. Movileanu, Explosion of gaseous ethylene–air mixtures in closed cylindrical vessels with central ignition, J. Hazard. Mater. 235 (2012) 108–115.
[23] M. Mitu, V. Giurcan, D. Razus, D. Oancea, Influence of initial pressure and vessel's geometry on deflagration of stoichiometric methane–air mixture in small-scale closed vessels, Energy Fuels 34 (2020) 3828–3835.
[24] B.W. Lei, J.J. Xiao, M. Kuznetsov, T. Jordan, Effects of heat transfer mechanism on methane-air mixture explosion in 20 L spherical device, J. Loss Prev. Process Ind 80 (2022) 104864.
[25] B. Lei, Q. Wei, R. Pang, J. Xiao, M. Kuznetsov, D. Jordan, The effect of hydrogen addition on methane/air explosion characteristics in a 20-L spherical device, Fuel 338 (2023) 127351.
[26] Y. Liang, B. Lei, S. Song, J. Xiao, M. Kuznetsov, T. Jordan, Numerical analysis of the distribution of combustion products from methane explosions in a full-scale tunnel using all-speed CFD code GASFLOW-MPI, Energy Sources, Part A: Recovery, Utilization, and Environmental Effects 45 (3) (2023) 7105–7121.
[27] Y. Liang, B. Lei, Y. Sun, W. Wang, Z. Liu, Shockwave and dynamic pressure propagation law of methane–air explosion in full-scale pipe network, Energy Sources, Part a: Recovery, Utilization, and Environmental Effects 44 (4) (2022) 9920–9934.
[28] J. Xiao, W. Breitung, M. Kuznetsov, H. Zhang, R. John, R. Reinhard, J. Thomas, GASFLOW-MPI: a new 3-D parallel all-speed CFD code for turbulent dispersion and combustion simulations: Part I: models, verification and validation, Int. J. Hydrogen Energy 42 (12) (2017) 8346–8368.
[29] J. Xiao, W. Breitung, M. Kuznetsov, H. Zhang, R. John, R. Reinhard, J. Thomas, GASFLOW-MPI: a new 3-D parallel all-speed CFD code for turbulent dispersion and combustion simulations Part II: first analysis of the hydrogen explosion in Fukushima daiichi unit 1, Int. J. Hydrogen Energy 42 (12) (2017) 8369–8381.
[30] J. Xiao, M. Kuznetsov, J.R. Travis, Experimental and numerical investigations of hydrogen jet fire in a vented compartment, Int. J. Hydrogen Energy 43 (2018) 10167–10184.
[31] J. Xiao, J.R. Travis, M. Kuznetsov, Numerical investigations of heat losses to confinement structures from hydrogen-air turbulent flames in ENACCEF facility, Int. J. Hydrogen Energy 40 (2015) 13106–13120.
[32] Turns SR. Introduction to combustion. NY, USA: McGraw-Hill Companies. New York; 1996, Vol. 287.
[33] J.J. Xiao, W. Breitung, M. Kuznetsov, H. Zhang, J.R. Travis, R. Redlinger, T. Jordan, GASFLOW-MPI: a new 3-D parallel all speed CFD code for turbulent dispersion and combustion simulations: Part I: models, verification and validation, Int. J. Hydrogen Energy 42 (2017) 8346–8368.
[34] H. Zhang, Y.B. Li, J.J. Xiao, T. Jordan, Detached Eddy simulation of hydrogen turbulent dispersion in nuclear containment compartment using GASFLOW-MPI, Int. J. Hydrogen Energy 43 (2018) 13659–13675.
[35] B. Franzelli, E. Riber, L.Y.M. Gicquel, T. Poinsot, Large eddy simulation of combustion instabilities in a lean partially premixed swirled flame, Combust. Flame 159 (2012) 621–637.
[36] E. Jq, H.J. Liu, X.H. Zhao, D.D. Han, Q.G. Peng, W. Zuo, T. Meng, R.Z. Qiu, Investigation on the combustion performance enhancement of the premixed methane/air in a two-step micro combustor, Appl. Therm. Eng 141 (2018) 114–125.
[37] C.K. Westbrook, F.L. Dryer, Prediction of laminar flame properties of methanol-air mixtures, Combust. Flame 37 (1980) 171–192.
[38] R.B. Bird, Transport phenomena, J. Electrochem. Soc 108 (78C) (1961).

[39] R. Siegel, J. Howell, Thermal radiation heat transfer, third ed., Hemisphere Publishing, Washington, 1992.
[40] S. Chandrasekhar, Radiative transfer, Dover ed., Dover Publications, New York, 1960.
[41] W.T. David, Radiation from flames, Nature 150 (1942) 407–408.
[42] M.A. Hadjipanayis, F. Beyrau, R.P. Lindstedt, G. Atkinson, L. Cusco, Thermal radiation from vapour cloud explosions, Process Saf. Environ. Protect 94 (2015) 517–527.
[43] E.M. Sparrow, Radiation heat transfer, first ed., Hemisphere Publishing, Washington, 1978.
[44] B. Zhang, X.Y. Chang, C.H. Bai, End-wall ignition of methane-air mixtures under the effects of CO_2/Ar/N_2 fluidic jets, Fuel 270 (2020) 117485.
[45] Z. Luo, L. Liu, F. Cheng, T. Wang, B. Su, J. Zhang, S. Gao, C. Wang, Effects of a carbon monoxide-dominant gas mixture on the explosion and flame propagation behaviors of methane in air, J. Loss Prevention Process Industries 58 (2019) 8–16.
[46] R. Li, Z. Luo, T. Wang, F. Cheng, H. Lin, X. Zhu, Effect of initial temperature and H_2 addition on explosion characteristics of H_2-poor/CH_4/air mixtures, Energy 213 (2020) 118979.
[47] The Engineering ToolBox. Surface Emissivity Coefficients 2003; [online] Available at: https://www.engineeringtoolbox.com/emissivity-coefficients-d_447.html [October 30, 2023].
[48] J. Nagy, Development and control of dust explosions, first ed., Marcel Deker Inc, New York, 1987.
[49] M.J. Sapko, A.L. Furno, J.M. Kuchta, Flame and pressure development of Large-scale CH_4-air-N_2 explosions: buoyancy effects and venting requirements, first, US Department of the Interior, Pittsburgh, 1976.
[50] B.Q. Lin, C.G. Jian, H. Zhang, The influence of heat dissipated in a conduit wall on the transmission characteristics of gas explosions, J. Chin. Univ. Min. Technol 38 (2009) 1–4.
[51] M. Kuznetsov, I. Matsukov, S. Dorofeev, Heat loss rates from hydrogen-air turbulent flames in tubes, Combust. Sci. Technol. 174 (2002) 75–92.